

基于光频梳的太赫兹器件面形测量技术研究

韩冰¹, 葛锦蔓^{1,2*}, 任心仪^{1,3}, 李小军², 刘佳², 闫明^{1**}, 曾和平^{1,3}¹华东师范大学精密光谱科学与技术国家重点实验室, 上海 200062;²中国空间技术研究院西安分院空间微波技术国家级重点实验室, 陕西 西安 710100;³华东师范大学重庆研究院, 重庆 401147

摘要 利用双光梳飞行时间法对小口径太赫兹天线及反射器面形进行了三维测量。实验中,单像素点测量时间为 8 μs ,纵向测量误差为 1.3 μm 。相较于传统的激光干涉法,双光梳法兼具了模糊距离大、测量精度高以及数据更新快等优势,为微波/太赫兹器件的面形测量提供了新途径。

关键词 测量; 太赫兹; 干涉; 相干; 成像系统

中图分类号 O436; TN247 **文献标志码** A

DOI: 10.3788/CJL202249.1704001

1 引言

微波和太赫兹 (THz) 天线、反射器等器件在通信、导航、遥感等领域具有重要的应用^[1]。激光跟踪测量技术是检测微波/THz 器件面形的重要手段之一,相比于全息法、摄影法等^[2-3],其具有更高的空间分辨率与检测精度,因此更适用于器件面形的精密测量^[4-5]。该方法基于激光干涉测距原理,测量精度可达 10^{-6} 量级^[5]。但是由于受到光学波长的限制,激光干涉法存在测量范围(量程)有限、更新速率低且需连续测量等问题^[4]。

光学频率梳 (optical frequency comb, 简称“光梳”) 的出现为光学精密测量提供了一种新的光源^[6]。光梳在频谱上由等间距分布的梳状频率线(梳齿)组成,且梳齿间具有稳定的相位关系及时频相干性。其中,任意一根梳齿的频率稳定度在 $10^{-12} \sim 10^{-15} \sqrt{\text{Hz}}$ 量级^[6],等效于一束单纵模稳频激光。这种相干性在时间域上则表现为载波包络相位稳定的超短脉冲序列。脉冲间的时间抖动在阿秒 (10^{-18} s) 量级^[6]。因此,光梳兼具了高的频率精度与高的时间分辨能力。

光梳与迈克耳孙干涉仪或空间光调制器相结合可以实现亚波长精度的测距及成像功能^[7-9],但是受到移动臂或调制器的限制,存在数据更新率低、动态范围有限等问题。2013 年,Pham 等^[8]利用空间光调制成像的方式,实现了基于光梳的物体面形检测。但是该方法受到调制器的限制,测量像素点少且耗时长,如 4×4 矩阵的测量时间为 1.7 s,误差为 3.5 μm ^[9]。

另一方面,基于光梳的双光梳干涉技术 (dual-comb interferometry) 逐渐发展成一种多功能精密测量手段。其原理是利用两台重复频率(即梳齿间距)具有微小差别的光梳在一个高速探测器上进行光外差探测,将光梳由光频域下转换至射频频域,再结合先进的射频仪器对光梳光场的强度、频率及相位进行精确测量^[10]。2009 年, Coddington 等^[11]提出并实验验证了一种基于双光梳干涉技术的测距方案,即双光梳测距 (dual-comb ranging) 技术。该方法集合了干涉法的高精度与脉冲飞行时间 (time-of-flight, TOF) 法的快速及模糊距离 (ambiguity range) 大的优势,在 60 ms 的采样时间内测距误差可达 5 nm,模糊距离达 30 km。随后,国内外研究者从光源、装置、探测以及实用性等方面对该技术进行了改进^[12-20]。近些年,该技术在测距中的优势被逐渐应用于光学成像领域。2018 年, Wang 等^[18]提出了光谱编码的双光梳三维形貌成像方案,纵向测量精度为 12 μm (光程为 114 mm),线数据更新率为 5 kHz。受限于色散元件及光谱带宽,该方法的空间分辨率及精度有限。2021 年, Vicentini 等^[19]提出了双光梳全息成像技术,利用两台电光光梳在相机感光面上的干涉探测实现了三维全息成像。但是受限于相机帧速,测量过程耗时过长。因此,双光梳技术的优势未能在成像应用中得到充分利用。此外,双光梳技术在小口径 THz 器件面形检测方面的应用尚无报道。

本文结合双光梳单点测距技术与高速二维振镜扫描法,对 THz 天线及反射器表面形貌进行了测量。实

收稿日期: 2021-11-08; 修回日期: 2021-12-11; 录用日期: 2021-12-27

基金项目: 国家自然科学基金(11904283)、空间微波技术国家级重点实验室稳定支持基金(HTKJ2020KL504013)

通信作者: *gjm129@163.com; **myan@lps.ecnu.edu.cn

验中,三维面形图像的单次扫描时间为 2 s,像素数为 2.5×10^5 ,即单像素扫描时间为 $8 \mu\text{s}$ 。纵向测量误差为 $1.3 \mu\text{m}$ (在 0.1 s 积分时间下可降至 5 nm),模糊距离可达 300 m。实验验证了双光梳测距成像在测量时间、精度以及动态范围等方面的优势,有望为高精度微波/THz 器件面形测量提供新的途径。

2 基本原理

本文中面形测量的实现是基于双光梳测距原理。其中,探测光梳(脉冲重复频率为 f_{r1} ,重复时间为 $T_{r1}=1/f_{r1}$)和本振光梳(重复频率为 f_{r2} ,重复时间为 $T_{r2}=1/f_{r2}$)存在着微小的重复频率差 $\Delta f=f_{r1}-f_{r2}$ 。其在时间域上的表现是本振脉冲以 $m \cdot \Delta T$ 的时间间隔对探测脉冲进行异步光学采样^[9],其中 m 为脉冲序数, ΔT 为采样步长,即

$$\Delta T = |T_{r1} - T_{r2}| = \frac{\Delta f}{f_{r1} f_{r2}} = \frac{\Delta f}{f_{r1}} \cdot T_{r2} \quad (1)$$

这里定义 $k = \frac{\Delta f}{f_{r1}}$,为光学采样中光学时间轴与测量时间轴之间的转换系数,其倒数 $1/k$ 即为光频与射频域的转换系数。待测样品表面的形貌起伏在探测脉冲中引入了延时差量 $\Delta\tau$,与实测双光梳干涉条纹移动量(Δt)的转换关系为 $\Delta\tau = \Delta t \cdot k$ 。

由脉冲飞行时间($\Delta\tau$)与空间距离(Δd)的基本关系,可知

$$\Delta d = v_g \cdot k \cdot \Delta t / 2, \quad (2)$$

式中: $v_g=c/n_g$ 为光脉冲在空气中的群速度,其中 n_g 为空气折射率, c 为真空光速。这里需要说明的是,实验中环境温度为 293 K,气压为 101.325 kPa,湿度为 50%,根据修正的 Edlén 公式^[21] 可得 $n_g = 1.000268151$ 。当 $\Delta\tau = T_{r1}$ 时,探测与本振脉冲在时间域是完全重合的,即一个重复周期。此时,双光梳测量时间(即单次测量时间)为 $\Delta t_{\text{measure}} = \frac{1}{\Delta f}$,相应的数据更新频率为 Δf ;重复周期内的最大非模糊距离为 $\Delta d_{\text{max}} = v_g \cdot \frac{T_{r1}}{2}$ 。测距技术的模糊距离直接限制了其在形貌成像应用中的纵向坐标测量范围(量程)。在双光梳测距技术^[10]中,更替探测与本振光梳的重复频率可以达到扩展模糊距离的目的,其原理与游标卡尺^[11]类似。此时限制量程的不再是光梳脉冲的重复周期(T_{r1} 或 T_{r2}),而是双光梳干涉条纹的重复周期($\frac{1}{\Delta f}$)。

因此,模糊距离可扩大为

$$\Delta D_{\text{max}} = \frac{v_g}{2\Delta f} \quad (3)$$

3 实验装置

实验装置采用两台近红外电光梳发生器(electro-optic comb,EOC)EOC 1 和 EOC 2 分别作为探测与

本振光源,如图 1(a)所示。电光梳发生器内含一个法布里-珀罗相位调制器和一个高频(25 GHz)信号源。信号源时钟同步于一台氢原子钟(秒稳为 10^{-13})。两台光梳的重复频率由各自信号源设定,分别为 $f_{r1} = 25 \text{ GHz}$ 和 $f_{r2} = f_{r1} + \Delta f = 25 \text{ GHz} + 0.5 \text{ MHz}$ 。为了减小相对频率/相位抖动,两台光梳的种子光源于同一台单频激光器。该种子光的中心波长为 1555 nm(对应频率 f_{cw} 为 192.79 THz),纵模线宽为 3 kHz。因此,两台光梳的梳齿频率分别表示为 $f_{\text{cw}} + n \cdot f_{r1}$ 及 $f_{\text{cw}} + n \cdot f_{r2}$,其中 f_{cw} 为连续激光器的重复频率, $f_{r2} = f_{r1} + \Delta f$, n 为整数,表示梳齿序数,取值范围为 $-N \sim N$ 。这里 $2N + 1$ 为单台光梳的总梳齿个数。两台光梳的光谱特性相似, -20 dB 处的光谱范围为 1542 ~ 1568 nm [图 1(b)],对应频谱宽度约为 3.22 THz,梳齿个数为 129。光谱仪在 0.02 nm 分辨率条件下可以清晰分辨光梳梳齿,如图 1(b)中插图所示。

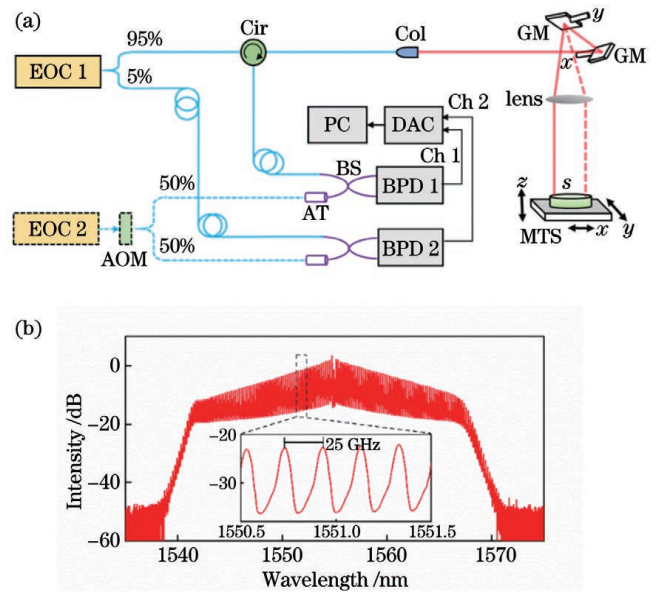


图 1 双光梳面形测量系统。(a)实验装置图;(b)电光梳输出光谱图

Fig. 1 Double-comb surface shape measuring system. (a) Experimental setup; (b) output spectrum of electro-optical comb

探测光梳 EOC 1 的输出光功率为 11 mW,本振光梳 EOC 2 的输出光功率为 2.7 mW。探测光(功率占比为 95%)经过光纤环形器(Cir)后由准直器(Col)耦合输出。在空间光路中,探测光经过高速扫描振镜组件(GM)后,经过焦距为 200 mm 的透镜直射待测样品(S)表面。样品置于多维平移台(MTS)上,用于调整纵向(z 轴)位移以及拓展成像范围。探测光被样品表面反射后,沿原路返回,被光纤准直器收集。返回的探测光被环形器导入分光比为 50:50 的光纤分束器(BS)。本振光(功率占比为 50%)经过衰减(AT)后,与返回的探测光在 BS 中合束,BS 的两个输出端分别接入平衡探测器(BPD 1)的正负输入端,探测器带宽

为 1.6 GHz。本振光与探测光在探测器上产生双光梳光外差拍频信号,高速数据采集卡(DAC)对信号采样、记录。平衡探测器有利于抑制两台光梳的共模强度噪声。同时,两台光梳的部分输出光在平衡探测器 BPD 2 上进行双光梳拍频,该拍频信号用作参考信号。两个平衡探测器的输出端与数据采集卡通道(Ch)连接。数据的采集和分析以及扫描振镜的控制均由个人计算机(PC)完成。实验中,为了避免双光梳测量中的频率混叠现象^[9,15],采用光声调制器(AOM)在本振光梳中引入频率偏移量 f_{AOM} 。因此,拍频信号在射频域上可以表示为 $f_{AOM} + n \cdot \Delta f$;在时间域上则表现为一组正弦函数波的叠加,其载波频率为 $f_{AOM} = 40$ MHz,包络重复频率为 $\Delta f = 0.5$ MHz。需要说明的是,系统中参考臂与测量臂光纤的长度相近且处于相同环境中,因此减少了光纤引入的测量误差。

4 实验结果与讨论

4.1 双光梳干涉条纹及拟合

为了验证系统的测量误差,首先选择一个平面镀银的反射镜作为待测件。图 2(a)展示了探测器 BPD 1 输出的双光梳干涉条纹,采样时间为 0.9 ms,数据采样率为 10^9 Sample/s。图 2(b)给出了 4 个周期的干涉信号。信号的重复周期(即两个干涉峰之间的时间间隔)为 $2 \mu\text{s}$,等于重复频率差的倒数($1/\Delta f$)。沿纵向(z 轴)移动待测件,可以实时地观测到干涉条纹在时间轴上的移动。该时间域的移动量(Δt)与待测件位移改变量(Δd)呈一一对应关系。探测光梳重复频率对应的模糊距离 Δd_{max} 为 6 mm;将本振光梳与参考光梳对调后,再次测量,可以将模糊距离扩大至 300 m^[11,17]。

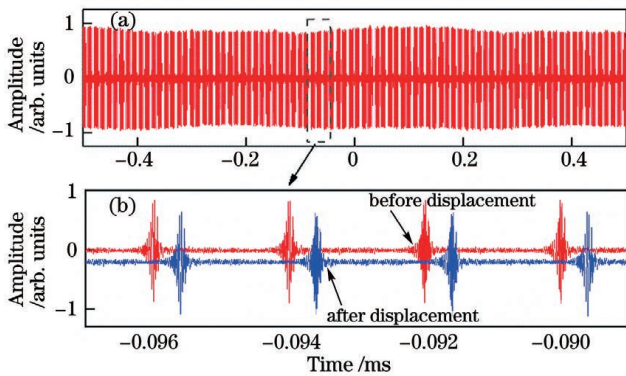


图 2 双光梳时域特性。(a)时域双光梳干涉序列;
(b)局部放大图

Fig. 2 Time domain characteristics of dual-comb. (a) Time domain dual-comb interferometric sequence;
(b) partial enlargement

为了准确地确定 Δt ,实验对干涉条纹进行了拟合。以图 3 为例,为了确定初始位置处于干涉条纹中心的时间坐标($t_1 = 0.02 \mu\text{s}$),首先对信号进行希尔伯特变换(Hilbert transform),获得干涉条纹的包络轮廓;

然后对轮廓进行洛伦兹拟合(Lorentz fit),求取拟合误差(σ_1)。图 4 的数据拟合结果为 $t_1 = 0.02 \mu\text{s}, \sigma_1 = 5 \times 10^{-5} \mu\text{s}$ 。同理,可以确定待测件移动后干涉条纹中心的时间坐标 t_2 与拟合误差 σ_2 ,并由此计算出时间差 $\Delta t = t_2 - t_1$ 以及相应误差 $\sigma_t = (\sigma_1^2 + \sigma_2^2)^{1/2}$ 。由式(2)得到相对位移 Δd 和位移误差值 σ_d 。需要指出的是,拟合误差与干涉信号信噪比(R_{SN})有关,信噪比越高,拟合误差越小^[9]。图 3 中干涉图案的信噪比为 6000,具体计算方法可参考文献[17]。

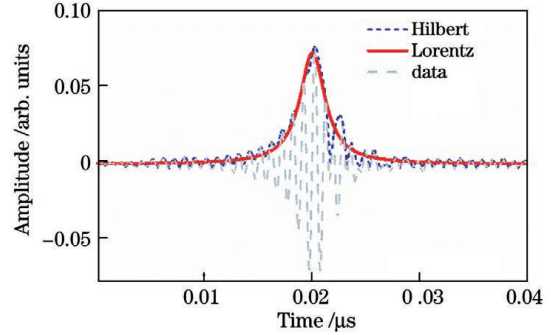


图 3 单周期双光梳干涉条纹

Fig. 3 Single-cycle dual-comb interferogram

4.2 误差测量

实验对装置的系统误差进行了评估。在待测件静止的情况下,记录时长为 0.6 s 的双路干涉条纹数据(包括 BPD 1 输出的待测信号及 BPD 2 输出的参考信号),将同周期($2 \mu\text{s}$)内的两路干涉信号时间差转换为位移差,并计算 Allen 方差^[10]。结果如图 4(a)所示。系统在测量时间为 $2 \mu\text{s}$ 即单周期条件下,测量误差为 $3.1 \mu\text{m}$;当测量时间为 80~100 ms 时,误差降至最小值,即 5 nm。随后测量误差受到光源相干时间、环境扰动和噪声的影响,呈上升趋势。图 4(b)给出了间断测量的 30 组重复性实验结果。每组测试用时

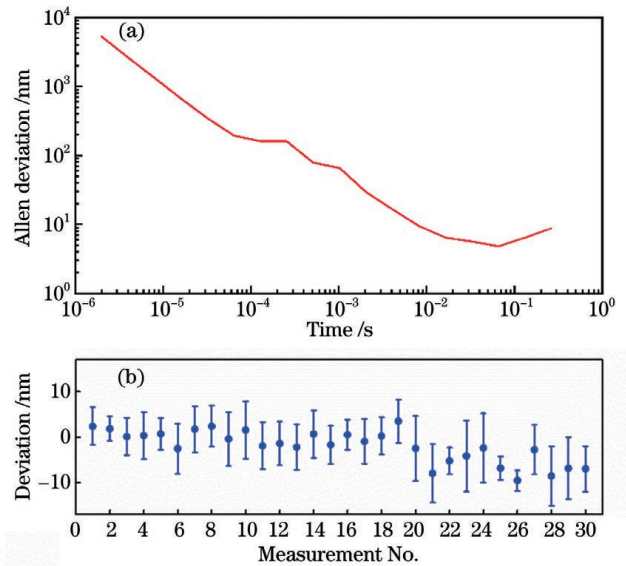


图 4 系统稳定性测试。(a)Allen 方差图;(b)误差图
Fig. 4 Test of system stability. (a) Allen deviation;
(b) deviation

30 min。在图 4(b)中,30 组数据的均值偏差量在 5 nm 以内,误差分布在 ± 10 nm 以内。实验结果表明,双光梳系统的纵向(z 轴)位移测量精度达纳米量级,且具有较好的可重复性和稳定性。

为了验证双光梳法在振镜高速扫描过程中的测距精度,实验利用振镜沿平面镜镜面内的一条直线对光束进行反复扫描(周期为 4 ms,扫描长度为 30 mm,对应 500 个数据点,即单像素扫描时间为 $8 \mu\text{s}$),同时记录双光梳纵向测距结果。图 5 给出了部分(10 组)测量结果。对 300 组单次扫描测量数据进行线性拟合后求标准方差,可得测量误差为 $(1.3 \pm 0.2) \mu\text{m}$,略高于静态测量误差值 [$0.9 \mu\text{m}$,测量时间为 $8 \mu\text{s}$,图 4(a)]。这说明高速振镜引入了一定的机械扰动。

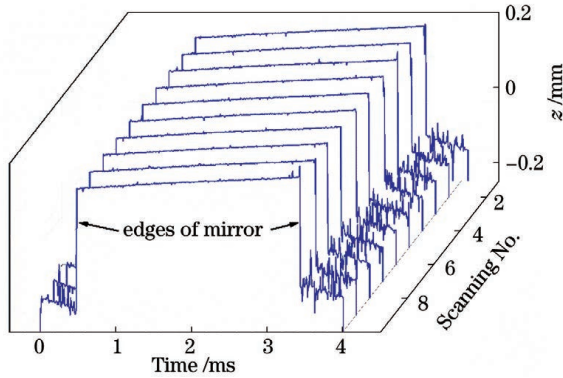


图 5 振镜扫描下的双光梳测量结果

Fig. 5 Dual-comb measurement result under galvanometer scanning

4.3 THz 器件面形检测结果

利用双光梳干涉系统对两款 THz 反射器面形进行了三维(3D)测量。通过高速振镜组(最高扫描频率 > 10 kHz)对样品表面进行点扫描成像,单次成像面积可达 $50 \text{ mm} \times 50 \text{ mm}$,点阵数为 500×500 ,耗时 2 s。扫描阵列中点间距(横向分辨率)设置为 $100 \mu\text{m}$,略大于光束在焦点处的光斑直径(约 $78 \mu\text{m}$)。图 6 给出了样品 1 表面反射的双光梳干涉条纹测量信号和参考信号。不同于平面反射镜的高反射率,待测样品表面反射率仅为 30%,对干涉测量信

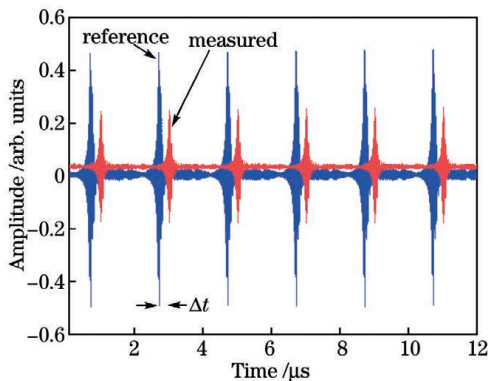


图 6 样品 1 表面反射的测量信号和参考信号

Fig. 6 Measured signal and reference signal reflected by surface of sample 1

号造成了一定程度的衰减。即便如此,图 6 中单周期干涉测量信号的信噪比仍大于 1000。

样品 1 为椭球面面形的 THz 反射器,如图 7(a)左上方插图所示,投影圆直径为 100 mm,曲面深度为 6 mm。图 7(a)为成像测量结果。由于基于扫描振镜的单次成像无法覆盖样品表面,因此图 7(a)为 4 组测量数据拼接的结果,各像素点的双光梳干涉信号的信噪比均值约为 2000 ± 400 ,单点在 z 轴方向上的测量误差约为 $1.3 \mu\text{m}$ 。这里的信噪比与样品表面光滑度及探测光束平行度有关。利用 Matlab 程序对数据进行 3D 曲面拟合,结果如图 7(b)所示,得出样品 1 的曲面平整度为 $34.78 \mu\text{m}$,拟合误差为 $19.84 \mu\text{m}^2$ 。

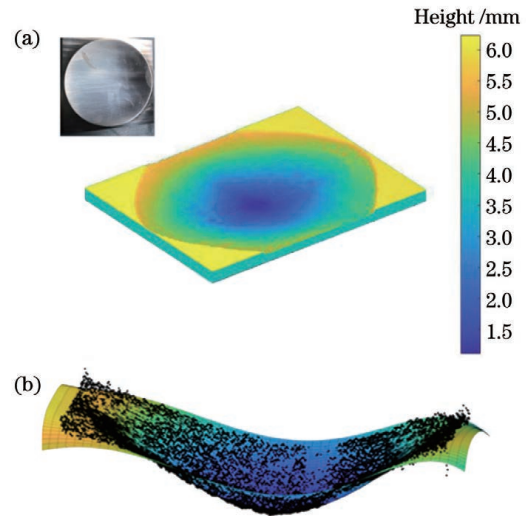


图 7 样品 1 的表面形貌。(a)天线样品 1 的 3D 形貌图(插图为实物图);(b)曲面拟合结果

Fig. 7 Surface morphologies of sample 1. (a) 3D topography of antenna sample 1 with physical picture shown in inset; (b) result of surface fitting

样品 2 为平面面形的 THz 天线样件,直径为 80 mm,其中心处为深度为 0.3 mm、直径为 20 mm 的凹坑,实物如图 8(a)左上方插图所示。图 8(a)为双光梳成像测量结果。考虑到样品结构特殊,仅选取样品 2 表面的一个平整区域[如图 8(a)虚线框所示]进行了平面拟合。拟合结果如图 8(b)所示,线平滑度为 $11.2 \mu\text{m}$,面平整度为 $5.85 \mu\text{m}$,拟合误差为 $0.02 \mu\text{m}^2$ 。该结果与扫描型三坐标仪的测量结果[面平整度为 $(7.1 \pm 2.0) \mu\text{m}$]一致。

4.4 分析与讨论

实验中,双光梳法测量单点位移的误差在 ± 10 nm 以内(测量时间为 0.1 s),但是成像视野受到了振镜扫描范围的限制($50 \text{ mm} \times 50 \text{ mm}$),因此,相较于全息法和摄影法等,该技术更适用于对面形测量精度要求更高的小口径微波/THz 器件^[9]。另一方面,双光梳法能够较好地同时满足实际应用对测量精度与速度的要求^[22]。例如,双光梳法对单像素点的测量时间仅为 $8 \mu\text{s}$,对应的像素更新频率达 125 kHz,此时位

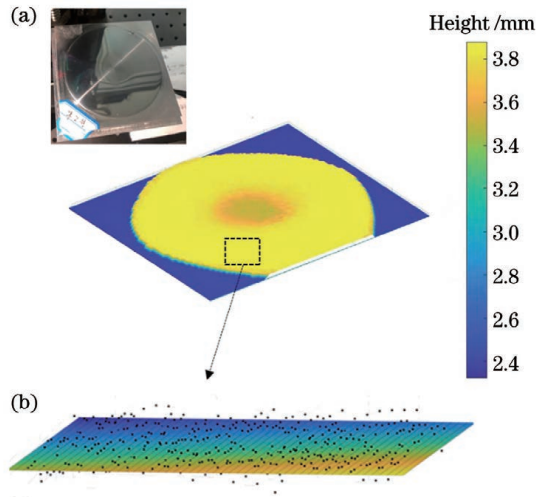


图 8 样品 2 的表面形貌。(a) 天线样品 2 的 3D 形貌图 (插图为实物图); (b) 曲面拟合结果

Fig. 8 Surface morphologies of sample 2. (a) 3D topography of antenna sample 2 with physical picture shown in inset; (b) result of surface fitting

移测量误差仅为 $1.3 \mu\text{m}$; 当测量时间增至 80 ms 时, 误差可降至 5 nm 。此外, 实验中采用了电光调制光梳, 有效避免了传统锁模光梳所带来的操作复杂、便携性差及成本高等问题^[23], 具有更好的实用性, 因此有望为高精度的微波/THz 器件面形检测提供新的平台。

5 结 论

采用双光梳飞行时间法, 对 THz 天线及反射器进行了形貌测量与三维形貌还原。曲面拟合结果显示, 样品 1 和 2 的平整度分别为 $34.78 \mu\text{m}$ 和 $5.825 \mu\text{m}$, 与商售三坐标仪的测量结果一致。对系统误差的测量与分析结果表明, 双光梳技术在纵向测量精度、模糊距离及更新速率等方面具有优势, 可应用于高精度、大动态范围的微波/THz 器件面形检测。

参 考 文 献

- [1] 汪赞, 孔德庆, 陈志平. 大型射电望远镜面形精度测量方法研究综述[J]. 天文研究与技术, 2020, 17(1): 52-59. Wang Z, Kong D Q, Chen Z P. Surface measuring methods of large antenna: a review [J]. Astronomical Research & Technology, 2020, 17(1): 52-59.
- [2] 马开锋. 高低温环境卫星天线形面变形的近景摄影测量与数据处理[D]. 北京: 中国矿业大学(北京), 2016: 1-4. Ma K F. Close-range photogrammetry and data processing of shape-surface deformation of satellite antenna under high-low temperature environments [D]. Beijing: China University of Mining & Technology, Beijing, 2016: 1-4.
- [3] 张德海, 梁晋, 唐正宗, 等. 基于近景摄影测量和三维光学测量的大幅面测量新方法[J]. 中国机械工程, 2009, 20(7): 817-822. Zhang D H, Liang J, Tang Z Z, et al. New measuring method of large size measurement based on close range photogrammetry and 3D optical measurement[J]. China Mechanical Engineering, 2009, 20(7): 817-822.
- [4] 吴广华. 智能化高精度天线面形测量系统关键技术研究[D]. 合肥: 合肥工业大学, 2017. Wu G H. Research on key technology in the intelligent and high-precision antenna shape-surface measurement system[D].

- Hefei: Hefei University of Technology, 2017.
- [5] 詹玉凤, 韩永伟, 宁锐, 等. 激光跟踪仪在飞机雷达天线面板安装精度测量中的应用[J]. 航空科学技术, 2012, 23(2): 47-49. Zhan Y F, Han Y W, Ning R, et al. Application of installation accuracy of measurement in aircraft radar antenna panel with laser tracker[J]. Aeronautical Science & Technology, 2012, 23(2): 47-49.
- [6] Diddams S A. The evolving optical frequency comb[J]. Journal of the Optical Society of America B, 2010, 27(11): B51-B62.
- [7] Kato T, Uchida M, Tanaka Y, et al. High-resolution 3D imaging method using chirped optical frequency combs based on convolution analysis of the spectral interference fringe[J]. OSA Continuum, 2019, 3(1): 20-30.
- [8] Pham Q D, Hayasaki Y. Interference imaging profilometry using optical frequency comb and compressive sensing [J]. Optics Express, 2013, 21(16): 19003-19011.
- [9] Hayasaki Y, Pham Q D. Optical frequency comb profilometry using a single-pixel camera [J]. Proceedings of SPIE, 2014, 9132: 913202.
- [10] Coddington I, Newbury N, Swann W. Dual-comb spectroscopy [J]. Optica, 2016, 3(4): 414-426.
- [11] Coddington I, Swann W C, Nenadovic L, et al. Rapid and precise absolute distance measurements at long range [J]. Nature Photonics, 2009, 3(6): 351-356.
- [12] Zhu Z B, Wu G H. Dual-comb ranging[J]. Engineering, 2018, 4(6): 772-778.
- [13] Lin B K, Zhao X, He M Z, et al. Dual-comb absolute distance measurement based on a dual-wavelength passively mode-locked laser[J]. IEEE Photonics Journal, 2017, 9(6): 17409614.
- [14] Zhang H Y, Wei H Y, Wu X J, et al. Absolute distance measurement by dual-comb nonlinear asynchronous optical sampling[J]. Optics Express, 2014, 22(6): 6597-6604.
- [15] Zhou S Y, Lin C, Yang Y T, et al. Multi-pulse sampling dual-comb ranging method [J]. Optics Express, 2020, 28(3): 4058-4066.
- [16] 崔鹏飞, 杨凌辉, 林嘉睿, 等. 飞秒光学频率梳在精密绝对测距中的应用[J]. 激光与光电子学进展, 2018, 55(12): 120011. Cui P F, Yang L H, Lin J R, et al. Application of femtosecond optical frequency comb in precise absolute distance measurement [J]. Laser & Optoelectronics Progress, 2018, 55(12): 120011.
- [17] 诸葛晶昌, 邢书剑, 高建树. 飞秒光频率梳的任意长绝对测距理论分析[J]. 光学学报, 2016, 36(1): 0112004. Zhuge J C, Xing S J, Gao J S. Theoretical analysis of arbitrary and absolute length measurement by using femtosecond optical frequency comb[J]. Acta Optica Sinica, 2016, 36(1): 0112004.
- [18] Wang C, Deng Z J, Gu C L, et al. Line-scan spectrum-encoded imaging by dual-comb interferometry[J]. Optics Letters, 2018, 43(7): 1606-1609.
- [19] Vicentini E, Wang Z, van Gasse K, et al. Dual-comb hyperspectral digital holography[J]. Nature Photonics, 2021, 15(12): 890-894.
- [20] Ren X Y, Xu B, Fei Q L, et al. Single-photon counting laser ranging with optical frequency combs [J]. IEEE Photonics Technology Letters, 2021, 33(1): 27-30.
- [21] Nsch G B, Potulski E. Measurement of the refractive index of air and comparison with modified Edlén's formulae[J]. Metrologia, 1998, 35(2): 133-139.
- [22] 葛锦蔓, 闫明, 谭庆贵, 等. 基于光梳的实时高分辨相位测量方法理论分析[J]. 中国激光, 2020, 47(11): 1104005. Ge J M, Yan M, Tan Q G, et al. Theoretical analysis of real-time high-resolution phase measurement method based on optical combs[J]. Chinese Journal of Lasers, 2020, 47(11): 1104005.
- [23] 陈旭, 金相宇, 王庆婷, 等. 基于压电陶瓷传感器以及多级温度反馈的小型化自适应双光梳[J]. 光学学报, 2021, 41(10): 1036001. Chen X, Jin X Y, Wang Q T, et al. A miniaturized adaptive dual-comb based on piezoelectric transducer and multi-stage temperature feedback[J]. Acta Optica Sinica, 2021, 41(10): 1036001.

Research on Surface Shape Measurement Technology of Terahertz Devices Based on Optical Frequency Comb

Han Bing¹, Ge Ginman^{1,2*}, Ren Xinyi^{1,3}, Li Xiaojun², Liu jia², Yan Ming^{1**}, Zeng Heping^{1,3}

¹ State Key Laboratory of Precision Spectroscopy Science and Technology, East China Normal University, Shanghai 200062, China;

² National Key Laboratory of Science and Technology on Space Microwave, China Academy of Space Technology, Xi'an 710100, Shaanxi, China;

³ Chongqing Institute, East China Normal University, Chongqing 401147, China

Abstract

Objective Microwave and terahertz (THz) devices, such as antennas and reflectors, are useful in communication, navigation, and remote sensing. The laser tracking and measuring technology plays an important role in characterizing microwave/THz devices, such as surface measuring. Laser tracking and measuring, which is based on laser interferometry, provides high spatial resolution and accuracy for precise surface topography measurements. However, it has limitations such as a limited dynamic range, a low update rate, and difficulty measuring absolute distance. A coherent light source with significantly advanced laser sensing and ranging is provided by an optical frequency comb, which is made up of a large number of equally spaced optical frequency lines (or comb teeth). Dual-comb-ranging interferometry, which uses two asynchronous optical combs to measure absolute distance, provides high precision, large ambiguity range, and high speed. This method, which does not use moving mirrors, demonstrates significant advantages in laser ranging and holographic imaging. The measurement process, however, can be time-consuming due to a camera's limited frame read-out speed. As a result, the benefits of dual-comb technology have not been fully exploited in imaging applications. Furthermore, dual-comb interferometry is yet to be used to characterize THz devices. In this paper, the dual-comb technique, combined with high-speed two-dimensional scanning mirrors, is applied to the surface measuring of THz devices. The measurement time per pixel for a three-dimensional (3D) image with 2.5×10^5 pixel is about 8 μ s. The longitudinal measurement error is 1.3 μ m (reduced to 5 nm at 0.1 s integration time), and the ambiguity range can reach 300 m. The experimental results show that dual-comb imaging is a useful and reliable tool for measuring the surface of microwave/THz devices with high precision.

Methods Two near-infrared electro-optic combs (EOC 1 and EOC 2) are used for constructing a dual-comb interferometer (Fig. 1). Each EOC contains a Fabry-Perot phase modulator driven by a radio frequency (RF) signal generator. The repetition frequencies of the two combs are set to $f_{r1} = 25$ GHz and $f_{r2} = f_{r1} + \Delta f = 25$ GHz + 0.5 MHz. Thus, the frequency of the n th comb line of the two combs can be expressed as $f_{cw} + n \cdot f_{r1}$ and $f_{cw} + n \cdot f_{r2}$, respectively, where $f_{r2} = f_{r1} + \Delta f$, f_{cw} is the repetition rate of the continuous laser, and n is an integer, ranging from $-N$ to N . Here, $2N+1$ are the total number of comb lines for a single comb. The spectral coverage of the two combs is similar, spanning from 1542 nm to 1568 nm at -20 dB (Fig.1), corresponding to 3.22 THz in spectrum width and 129 comb lines. The EOC 1 has an output power of 11 mW, while the EOC 2 has a power of 2.7 mW. The detection light is sent to a high-speed scanning galvanometer (GM) after passing through a fiber optic circulator (Cir) and a collimator (Col), and then hits the surface of a sample (S) that is placed on a 3D translation platform for adjusting the longitudinal (z -axis) displacement and expanding the imaging view. The reflected light propagates along the original beam path and then combines the local oscillator light (EOC 2) with a 50/50 fiber beam splitter (BS). The common-mode noise is then suppressed using the balanced photo-detector (BPD 1, bandwidth of 1.6 GHz). A data acquisition card (DAC) records the detection signal at a sample rate of 2.5×10^8 Sample/s. Note that, to avoid frequency aliasing in dual-comb measurement, an acoustic-optical modulator (AOM) is used to introduce a frequency offset at f_{AOM} (40 MHz) to the local comb (EOC 2). Thus, the beat frequency signal in the RF domain can be expressed as $f_{AOM} + n \cdot \Delta f$. It should also be noted that the optical fibers of the reference and measuring arms have similar lengths when placed in the same environment to minimize the fluctuation introduced by the fibers.

Results and Discussions An ellipsoidal THz reflector's imaging results (sample 1) are shown (Fig. 7). The sample projection plane has a diameter of 100 mm and a depth of 6 mm. The mean signal-to-noise ratio of each pixel is about 2000 ± 400 , and the measurement error in the z -axis direction is about 1.3 m, depending on the smoothness and shape of the sample surface (Fig. 7). We perform 3D surface fitting based on the data and the results (Fig. 7) show that the sample surface flatness is 34.78 μ m with a fitting error of 19.84 μ m².

Another sample, a planar THz antenna (sample 2), with a diameter of 80 mm and a concave pit in the center with a diameter of 20 mm and a depth of 0.3 mm, is measured (Fig. 8). A flat area of the surface is fitted, yielding the line smoothness of $11.2\ \mu\text{m}$, the plane flatness of $5.85\ \mu\text{m}$, and the fitting error of $0.02\ \mu\text{m}^2$ (Fig. 8), which are consistent with the results obtained by a contour measuring system, e. g., plane flatness of $(7.1 \pm 2.0)\ \mu\text{m}$. The uncertainty of a single-point measurement in the experiment is within $\pm 10\ \text{nm}$ (measurement time of 0.1 s), but the scanning motion of the galvanometer introduces additional fluctuations into the measurement, resulting in a measurement error of $(1.3 \pm 0.2)\ \mu\text{m}$ (acquisition time of $8\ \mu\text{s}$) for 3D imaging. Nonetheless, the dual-comb method holds great promise for the surface measuring of microwave/THz devices due to its high data update rate (125 kHz) and micrometer-level precision.

Conclusions The dual-comb time-of-flight method is used in this paper to measure the three-dimensional shapes of small aperture terahertz antennas and reflectors. The measurement time for a single pixel in the experiment is $8\ \mu\text{s}$, and the longitudinal measurement error is $1.3\ \mu\text{m}$. When compared to the traditional laser interferometry, the dual-comb method has the advantages of a large ambiguity range, high measurement accuracy, and a fast data update rate, making it promising for surface measurements of terahertz reflectors and microwave antennas.

Key words measurement; terahertz; interference; coherence; imaging systems